STABILITY OF ARMOR UNITS COVERING RUBBLE MOUND OF COMPOSITE BREAKWATERS AGAINST A STEADY OVERFLOW OF TSUNAMI

Jun Mitsui[1], Akira Matsumoto[1], Minoru Hanzawa[1] and Kazuo Nadaoka[2]

This paper presents a simple and highly accurate stability estimation method for armor units covering breakwater rubble mounds against tsunami overflow. In this method, overflow depth is used to represent the external force. This enables an easier and more robust estimation of the required mass of the armor units than the conventional method based on flow velocity. This method takes into account the influence of the impingement position of the overflow jet and the influence of harbor-side water depth, both of which are important factors for armor stability. Numerical computation is also carried out aiming at the establishment of a stability analysis method for armor units. The validity of the computation method is confirmed by comparing the measured current field. The stability of armor units is investigated by computing the hydraulic force acting on each armor unit.

Keywords: tsunami; overflow; armor unit; stability; harbor-side; breakwater

INTRODUCTION

Numerous composite breakwaters were severely damaged by the 2011 Off the Pacific Coast of Tohoku Earthquake Tsunami. One of the causes of failure was a scouring of the rubble foundation and subsoil on the harbor-side of breakwaters due to the overflow. This was a formerly inconceivable type of failure (Ministry of Land, Infrastructure, Transport and Tourism 2013). One possible countermeasure is the placement of a widened protection using additional rubble stones behind the breakwater to prevent the sliding of the caisson. Installing armor units on the rubble mound on the harbor-side would also be required to prevent the scouring around the rubble mound (Fig. 1).

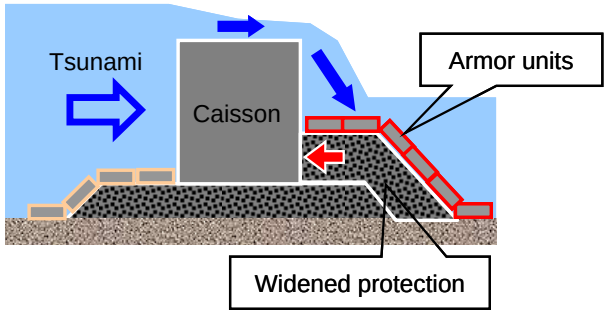

Figure 1. Countermeasure against tsunami of breakwaters.

The Isbash formula (Coastal Engineering Research Center 1977) has been applied previously as the method to determine the mass of armor units. The required mass calculated by this formula is proportional to the sixth power of the flow velocity near the armor unit. This causes a practical problem that the required mass is too sensitive to variations in the estimated flow velocity. In this context, establishment of a more practical method to determine the mass of armor units is an urgent issue toward the achievement of resilient breakwaters against tsunami.

This paper presents a simple and highly accurate method which can estimate the stability of armor units by using the overflow depth instead of the flow velocity. Hydraulic model experiments in a wide range of conditions were conducted to extract key factors for armor stability. Empirical formulae were then derived based on the experimental results.

Numerical analysis was also carried out aiming to evaluate the stability for cases beyond the range of experimental conditions. First, the flow field on the harbor-side of the breakwater was reproduced. The computation method was validated by comparing the measured and computed current fields. The stability of armor units was then investigated by computing the hydraulic force acting on each armor unit.

[1] Technical Research Institute, Fudo Tetra Corporation, 2-7, Higashi-nakanuki, Tsuchiura, Ibaraki, 300-0006, Japan, jun.mitsui@fudotetra.co.jp; akira.matsumoto@fudotetra.co.jp; minoru.hanzawa@fudotetra.co.jp
[2] Mechanical and Environmental Informatics, Tokyo Institute of Technology, 2-12-1, O-okayama, Meguro-ku, Tokyo, 152-8552, Japan, nadaoka@mei.titech.ac.jp

HYDRAULIC MODEL EXPERIMENTS

Experimental setup

Experiments were carried out in a 50 m long, 1.0 m wide, and 1.5 m deep wave flume as shown in Fig. 2. A horizontal mortar seabed was partitioned into two sections along the length, and a breakwater model was installed in one 50 cm wide waterway. A submersible pump and discharge port were located on the harbor-side and sea-side of the breakwater model respectively to generate a steady overflow. The capacity of the pump was 4 m^3/min. A water level difference was generated between the inside and outside of the breakwater by operating the pump. The height of the sea-side water level could be changed by varying the height of the overflow weir installed on the sea-side of the breakwater model. The height of the overflow weir could be varied in a range of 0 to 50 cm. A vent hole with a diameter of about 25 mm was provided in the partition wall close behind the caisson to maintain the space between the caisson and overflow nappe in ambient atmospheric pressure conditions.

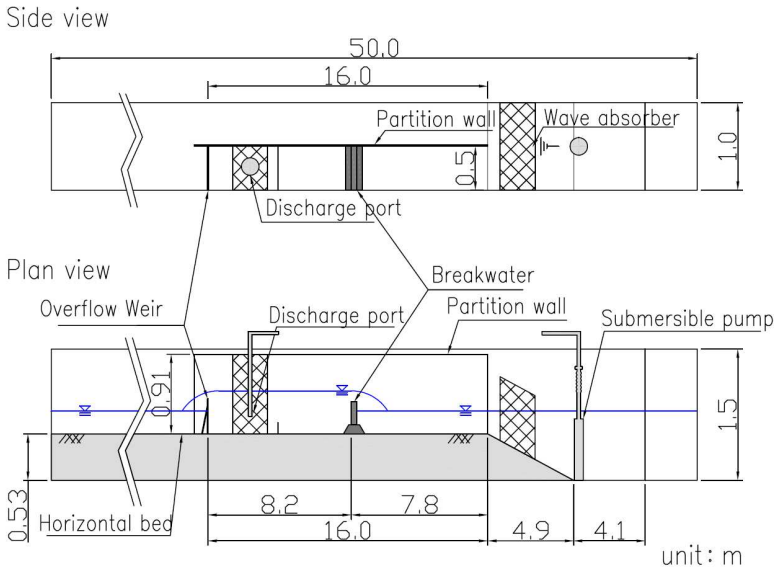

Figure 2. Test setup in the flume.

A schematic layout of the breakwater model is shown in Fig. 3. The model scale is 1/50. Experiments were carried out by changing the shape of the harbor-side rubble mound, the harbor-side water level, and the shape and mass of the armor units. Two kinds of flat-type armor blocks and wave-dissipating blocks were used in the experiments as shown in Fig. 4. The armor block with five holes is a recently developed block named “Permex” produced by refining the “X-block”. The large holes in the block have been found to contribute to high stability against wave action due to the reduction of the uplift force (Hamaguchi et al. 2007, Kubota et al. 2008). The caisson model was made of wood and was fixed with a weight so that it would not be moved by tsunami action since this study was focused on the stability of armor units.

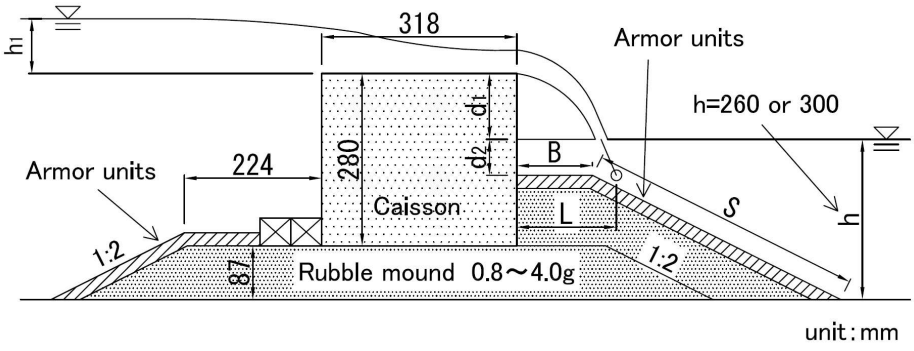

Figure 3. Schematic layout of the tested breakwater.

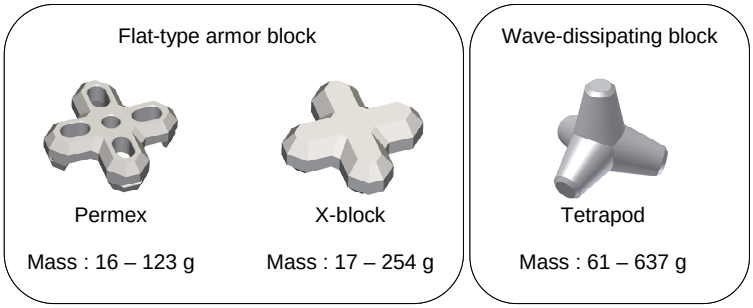

Figure 4. Armor units used in the experiments.

The duration time of the steady overflow of tsunami was set to 127 s (15 minutes in the prototype scale) to simulate the actual event observed in Hachinohe port during the Tohoku tsunami on March, 11th in 2011. As it took about 60 s until the water level achieved a steady state from the start of operating the pump, the total operation time of the pump was set to 187 s. The stability limits of the armor units were examined by increasing the overflow depth in increments of 1 cm. The overflow depth was defined as the difference between the sea-side water level (measured at 2 m on the offshore side from the front of the caisson) and the crest height of the caisson. The harbor-side water level was measured at 2 m on the onshore side from the rear wall of the caisson. The section was not rebuilt after tsunami attack with each overflow depth. The number of the moved armor units was counted as an accumulated number. The damage to armor units were defined using the relative damage N_0, which is the actual number of displaced units related to the width of one nominal diameter D_n (Van der Meer 1988). The nominal diameter D_n is the cube root of the volume of the armor unit. In this study, $N_0 = 0.3$ was applied as the criterion of damage.

Feature of the damage by tsunami overflow

Fig. 5 is a snapshot of the tsunami overflow in the experiment. As soon as the armor blocks at the slope section were washed away, the scouring of the rubble mound progressed rapidly and reached to the sea bottom within about 1 minute (7 minutes in the prototype scale). Though widened protection using additional stones exhibits a function to delay scouring, the damage expands rapidly if the armor units are washed away and the rubble mound is exposed. This is one of the features of damage by tsunami overflow.

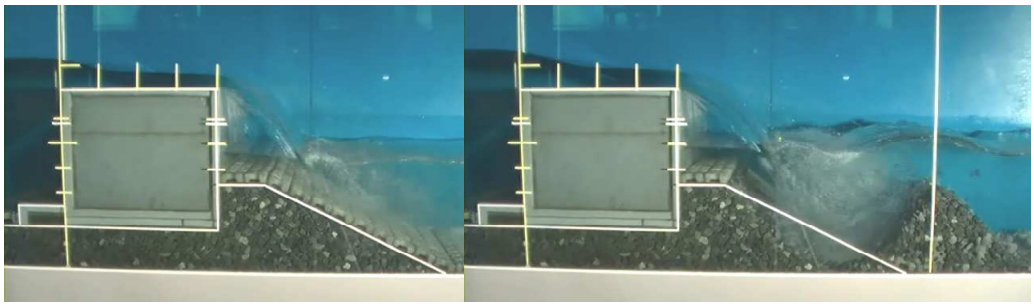

Figure 5. Snapshot of tsunami overflow.

Influence of impingement position of overflow jet

The impingement position of the overflow jet will change with various factors such as the shape of the harbor-side mound and the overflow depth. The influence of the impingement position on armor stability was examined by changing the crown width of the harbor-side mound. Fig. 6(a) shows an example of the stability test results. In this condition, the overflow jet impinged on the slope section when the number of armor units on the crown section was one or two, whereas it impinged on the crown section in the case of more than four units on the crown section. The cases in which the jet impinged on the slope section showed higher stability than the cases of impingement on the crown section. This shows that impingement position largely affects the armor stability. Because the effect of the impingement position depended on the structural conditions such as the shape of the armor units

and the presence or absence of widened protection, it is necessary to incorporate properly this effect into the estimation of the armor stability.

Influence of harbor-side water level

When a tsunami overflows the caisson, the discharged water from the rear end of the caisson accelerates during the freefall above the water surface, and decelerates under the water surface due to diffusion. Therefore, the stability of armor units should decrease as the crown height of the caisson above the harbor-side water level increases. Also, it should increase as the submerged depth above the armor units increases. Fig. 6(b) shows a comparison of the stability test results with two different harbor-side water levels. On the whole, the results of deep-water cases showed higher stability than those of shallow-water cases.

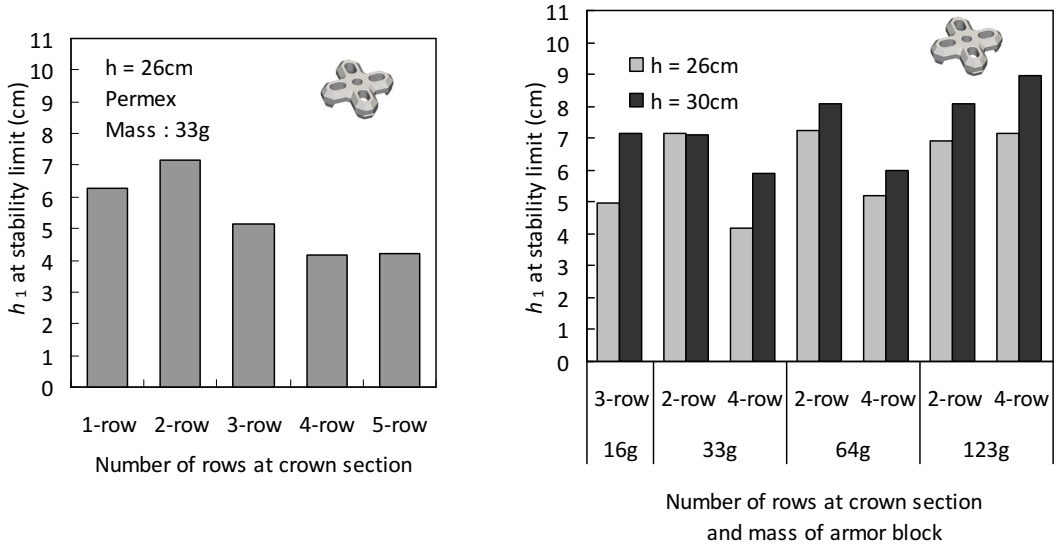

(a) Influence of impingement position (b) Influence of harbor-side water level

Figure 6. Influence of impingement position and harbor-side water level on the overflow depth h_1 at stability limits.

Failure modes of armor units

Two failure modes for flat-type armor blocks were observed in the experiments. One was an overturning mode in which armor blocks near the impingement position overturned. The other was a sliding mode in which all the blocks on the slope section slid together. Fig. 7 shows the relationship between the nominal diameter of the armor block D_n and the overflow depth h_1 on the occurrence of damage. In the cases of overturning mode, the overflow depth at the occurrence of damage was almost proportional to the nominal diameter D_n. On the other hand, in the cases of sliding mode, it had only small dependence on D_n. These results suggest that enlargement of the block size causes an increase in the acting force as much as the increase in the resistance force with regard to the sliding mode. For the wave-dissipating blocks, almost every failure pattern was that of blocks near the impingement position being displaced individually.

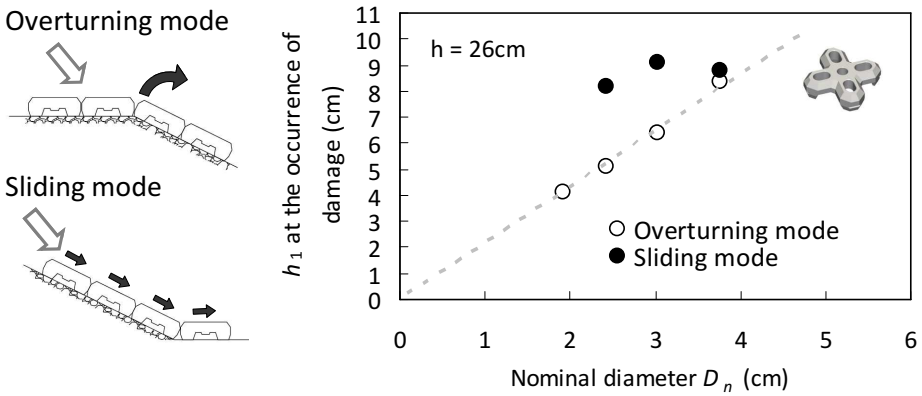

Figure 7. Relationship between the nominal diameter D_n and the overflow depth at the occurrence of damage by each failure mode.

Performance of the wave-dissipating concrete blocks

A characteristic of the wave-dissipating blocks installed in the two layers is that scouring becomes hard to progress rapidly even when many blocks displaced. The reasons are considered to be the following: (1) it takes a longer time before the rubble stones are exposed since they are covered with two layers, (2) displaced blocks piled up behind the impingement position prevent the progress of the scouring by staying interlocked without being washed away. Avoiding the rapid progress of scouring is important from the viewpoint of resilience of a breakwater in the prevention of large scattering of the caisson (Arikawa et al. 2013). The widened protection mound covered with wave-dissipating blocks may provide such resilience.

STABILITY ESTIMATION METHOD

Derivation of stability formulae

Two empirical formulae for the stability estimation were derived based on the experimental results mentioned above. The overflow depth was used in the formulae to represent the external force. The overflow depth of the stability limit corresponding to each failure mode was obtained by the two formulae. The final stability limit was determined by the severer one. The formulae for the overturning mode and sliding mode are expressed as follows:

$$\text{Overturning mode :} \qquad \frac{h_1}{(S_r-1)D_n} = N_{S1} = f\left(\frac{B}{L}, \frac{d_2}{d_1}\right) \tag{1}$$

$$\text{Sliding mode :} \qquad \frac{h_1}{(S_r-1)S} = N_{S2} = f\left(\frac{d_2}{d_1}\right) \quad \text{for} \quad \frac{B}{L} \le 1.1 \tag{2}$$

where, h_1 is the overflow depth, S_r is the specific gravity of concrete with respect to seawater, S is the slope length of the harbor-side rubble mound, N_{S1} and N_{S2} are the stability numbers, B is the crown width of the harbor-side mound, L is the impingement position of the overflow jet, d_1 is the crown height of the caisson above the harbor-side water level, and d_2 is the submerged depth above the armor units (regarding the definition of symbols, see Fig. 3). Stability numbers N_{S1} and N_{S2} are functions of B/L and d_2/d_1, which are the parameters representing the influence of the impingement position and the harbor-side water level respectively. The stability is determined only by Eq. (1) if B/L is larger than 1.1 since failure by sliding mode does not occur when the overflow jet impinges on the crown section. Similarly, the stability of wave-dissipating blocks is also determined only by Eq. (1).

For the overturning mode, the overflow depth h_1 represents the acting force on armor units, whereas the nominal diameter of armor units D_n represents the resistance force as shown in Eq. (1). For the sliding mode, on the other hand, the slope length S is used to represent the resistance force as shown in Eq. (2). this is because the resistance force should be represented by the total length of the blocks on the slope as the whole blocks on the slope section slide together in the sliding mode. As a

result, the overflow depth of the stability limit in the sliding mode is not dependent on the block size as can be seen from Eq. (2). This corresponds with the experimental results described above (see Fig. 7).

Determination of stability numbers

Fig. 8 shows the influence of the impingement position by plotting the stability number N_{S1} against B/L. The conditions of water depth are almost at the same level (d_2/d_1 = 0.47 to 0.66). The damage data with sliding mode is excluded in the figure to reveal the stability limit of overturning mode. The stability limit is expressed in a single line as a function of B/L regardless of the mass of the block. Also, the difference in the stability due to the impingement position appears clearly. Fig. 9 shows the influence of the harbor-side water depth by plotting the N_{S1} against d_2/d_1. The data on the conditions of $B/L > 1.0$ is used. The stability tends to increase as d_2/d_1 increases.

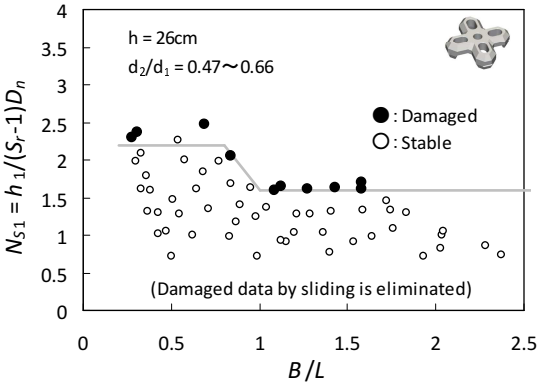

Figure 8. Influence of B/L on N_{S1}.

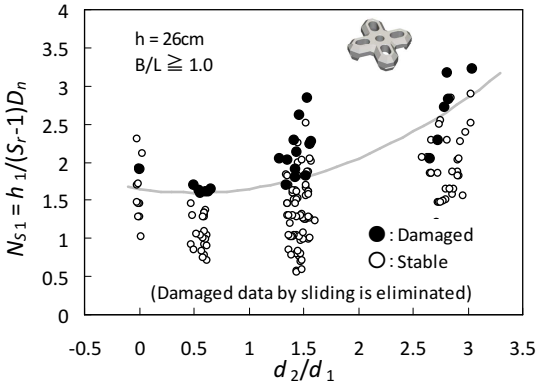

Figure 9. Influence of d_2/d_1 on N_{S1}.

Fig. 10 shows the stability numbers N_{S1} and N_{S2} for flat-type armor blocks determined through all the test results. Different lines are used according to the B/L in Fig. 10(a). When B/L is between 0.8 and 1.0, the value is obtained by linear interpolation. The stability of the Permex is higher than that of the X-block for both failure modes. The stability number for the wave-dissipating block is shown in Fig. 11. In the case of the wave-dissipating block, the influence of the impingement position was different from the case of the flat-type armor blocks. Namely, the cases in which the jet impinged on the crown section showed higher stability than the cases of impingement on the slope section. This result was reflected in Fig. 11.

Fig. 12 shows a comparison of the estimated overflow depth of stability limit with the damaged overflow depth in the experiments. The estimated results are on the safe side as a whole, and they show good agreement for both failure modes.

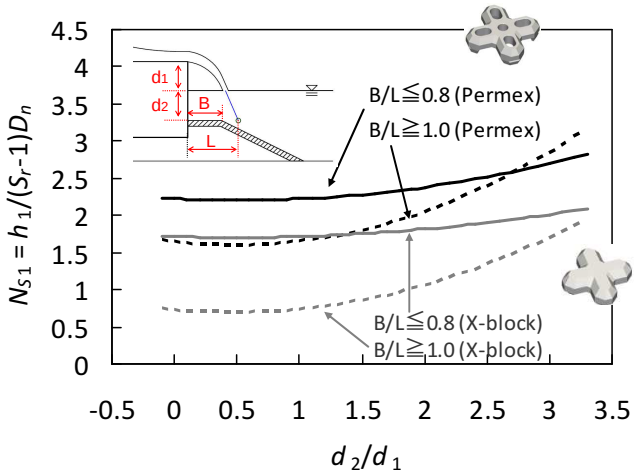

(a) N_{S1} (for overturning mode)

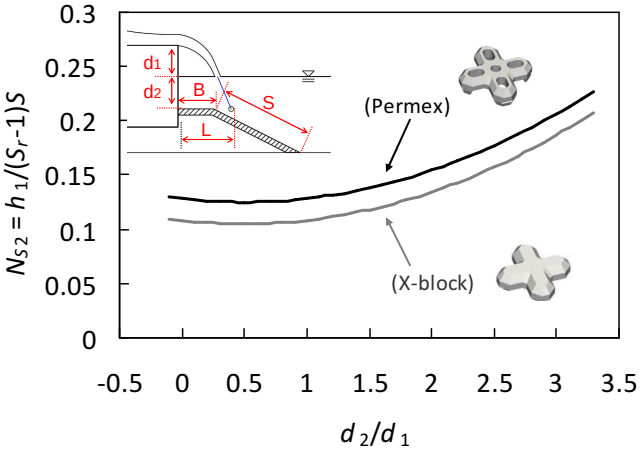

(b) N_{S2} (for sliding mode)

Figure 10. Stability numbers for flat-type armor blocks.

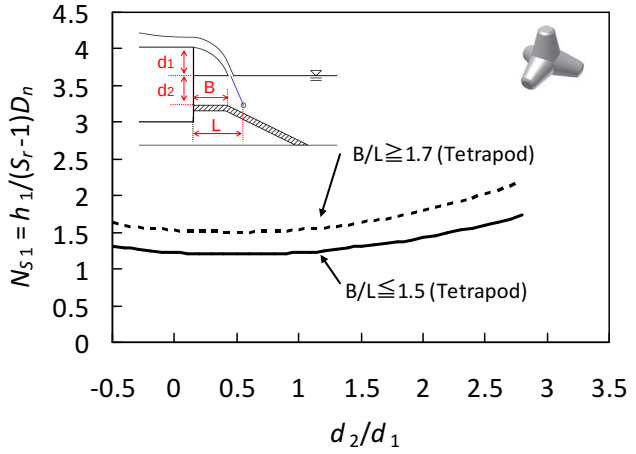

Figure 11. Stability numbers for wave-dissipating block.

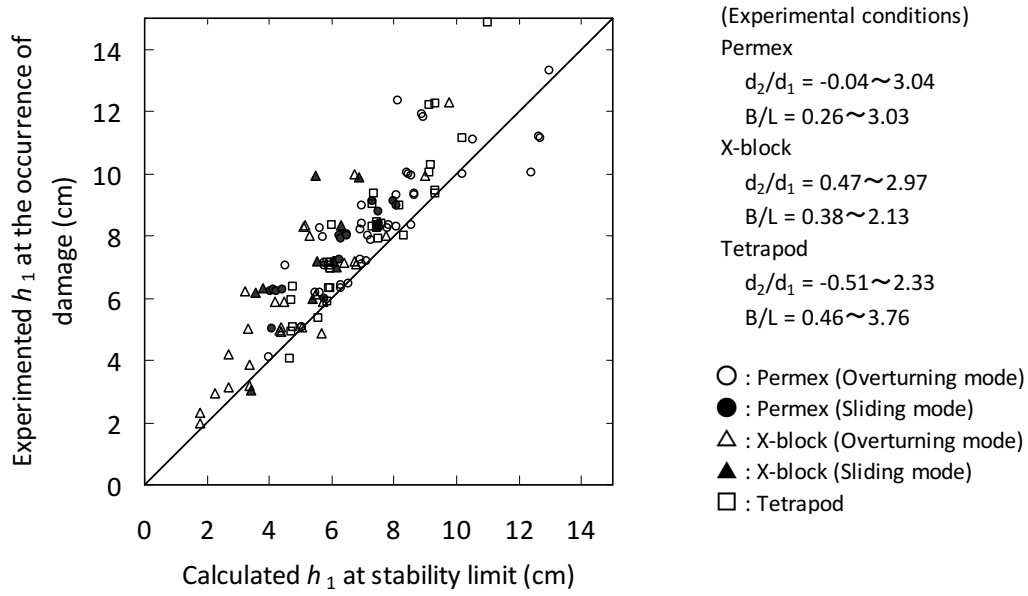

Figure 12. Calculated and experimented overflow depth of the stability limit.

Calculation method of the impingement position *L*

It is necessary to calculate the impingement position L to apply the estimation method. It can be calculated approximately using the overflow depth h_1 as shown below. The definition of each symbol is shown in Fig. 13.

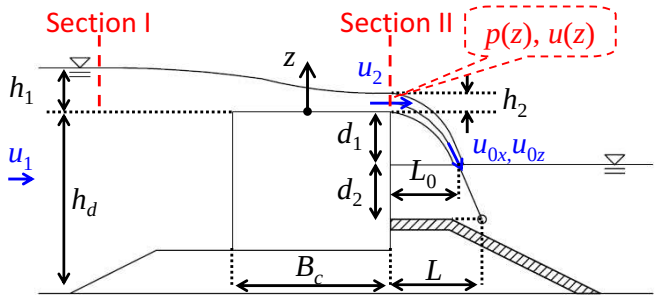

Figure 13. Definition of the symbols used in the calculation of the impingement position.

The overflow discharge per unit width q is calculated by using the Hom-ma formula (Hom-ma 1940b):

$$q = 0.35 h_1 \sqrt{2gh_1} \tag{3}$$

where g is the acceleration due to gravity. The application condition in this formula is $h_1/B_c < 1/2$. The effect of the approaching velocity u_1 can be disregarded if $h_1/h_d < 0.5$ (Hom-ma 1940a). The water depth above the caisson at the rear end of the caisson h_2 and the cross sectional averaged flow velocity u_2 are calculated according to Hom-ma (1940a) as shown below.

Applying the Bernoulli's theorem to Sections I and II yields following relation:

$$h_1 = z + \frac{p_{(z)}}{\rho g} + \frac{u_{(z)}^2}{2g} \tag{4}$$

where, z is the height measured from the top of the caisson, and $p_{(z)}$, $u_{(z)}$ are the pressure and the flow velocity at Section II, respectively. The overflow discharge q is obtained by integrating the flow velocity $u_{(z)}$ as follows:

$$q = \int_0^{h_2} \sqrt{2g\left(h_1 - z - \frac{p_{(z)}}{\rho g}\right)}\,dz \tag{5}$$

If the pressure distribution $p_{(z)}$ is obtained, h_2 can be calculated using Eq. (3) and Eq. (5). The pressure distributions were assumed as the following triangle distributions:

$$\begin{aligned} p_{(z)} &= \rho g\left(h_2 - z\right) \quad \text{for} \quad h_2/2 \le z \le h_2 \\ p_{(z)} &= \rho g z \quad \text{for} \quad 0 \le z \le h_2/2 \end{aligned} \tag{6}$$

Using Eq. (3), Eq. (5), and Eq. (6), one obtain Eq. (7):

$$0.35h_1\sqrt{2gh_1} = \sqrt{2g}\left\{-\frac{1}{3}\left[\sqrt{\left(h_1 - h_2\right)^3} - \sqrt{h_1^3}\right] + \sqrt{h_1 - h_2}\,\frac{h_2}{2}\right\} \tag{7}$$

The relationship between h_1 and h_2 are solved numerically with Newton's method as follows:

$$h_2 = 0.42h_1 \tag{8}$$

In this study, the following relationship was used considering its suitability to the experimental results:

$$h_2 = 0.45h_1 \tag{9}$$

The center of trajectory of the overtopped water was then obtained under the following assumptions:

- The overtopped water discharges horizontally from the rear end of the caisson at the flow velocity $u_2 = q/h_2$.
- The trajectory of the overflow nappe above the water surface is a parabola.
- The trajectory of the water below the water surface is a straight line.

The landing position of the overtopped water on the harbor-side water surface, L_0, and the flow velocity u_{0x}, u_{0z} are calculated as follows:

$$L_0 = u_2\sqrt{\frac{2\left(d_1 + h_2/2\right)}{g}} \tag{10}$$

$$u_{0x} = u_2, \quad u_{0z} = \sqrt{2g\left(d_1 + h_2/2\right)} \tag{11}$$

The impingement position L was thus obtained as follows:

$$L = L_0 + \frac{u_{0x}}{u_{0z}}d_2 \tag{12}$$

NUMERICAL ANALYSIS

Numerical analysis was carried out aiming to evaluate the stability in cases beyond the range of experimental conditions since the stability estimation method mentioned above has a range of applicable conditions even though it is based on experiments conducted in a wide range of conditions. First, the computation method of the flow field at the harbor-side of the breakwater was investigated. The method was validated by comparing the measured and computed flow field. Then the stability of the armor units was investigated by computing the hydrodynamic force acting on each armor unit.

Computation method

With regard to the numerical computation of the tsunami overtopping the caisson, Mitsui et al. (2012) adequately reproduced the laboratory experiment of a impinging bore-like tsunami by using the VOF method implemented in the OpenFOAM (OpenCFD Ltd.) CFD model. In the case of the steady overflow of tsunami, however, the computation result using VOF method did not reproduce well due

to the excessive entrainment of air into the impinging jet. Bricker et al. (2013) pointed out that this model overestimates the eddy viscosity at the air-water interface, and that it can be improved by neglecting all the turbulence in the air phase. In this study, the overflow jet above the water surface and the flow field on the harbor-side were solved separately to avoid excessive entrainment of air. A schematic diagram of the computation method is shown in Fig. 14.

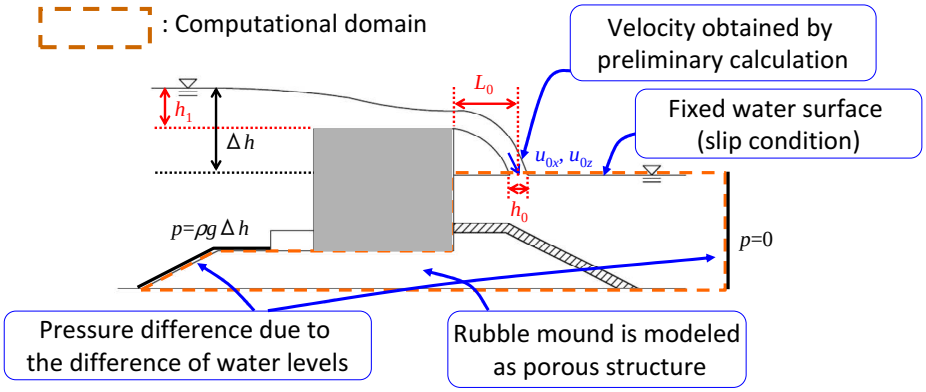

Figure 14. Schematic diagram of the computation method

The flow field under the water surface on the harbor-side was solved by a single-phase model. An incompressible flow solver within the OpenFOAM was used. The governing equations were the Reynolds-Averaged Navier-Stokes (RANS) equation and the continuity equation. The Finite Volume Method with an unstructured grid was used to reproduce the complicated shape of the armor blocks. The computational domain was cross-sectional 2-dimensions, and the standard grid size was set to 2 mm. In the cases of computing the fluid forces acting on the armor blocks, the grid was subdivided into 3-dimensions. The grid size around the block was set to about 1 mm so that the block shapes could be reproduced in detail.

The flow velocity u_{0x}, u_{0z} at the harbor-side water surface were given as boundary conditions. The velocity and the landing position of the overtopped water L_0 were obtained by preliminary calculation as shown in the previous chapter. The width of the water jet at the water surface h_0 was calculated as:

$$h_0 = \frac{q}{u_{z0}} \tag{13}$$

The water surface on the harbor-side was assumed as a fixed boundary. The rubble mound was modeled as a porous structure to reproduce the seepage flow under the caisson. The hydraulic flow resistance **R** in the porous medium was expressed by a Dupuit-Forchheimer relationship as shown below:

$$\mathbf{R} = -\left(\alpha \mathbf{U} + \beta |\mathbf{U}| \mathbf{U}\right) \tag{14}$$

where, **U** is the flow velocity vector, α is the laminar resistance coefficient and β is the turbulent resistance coefficient. These coefficients were expressed using the empirical formulae by Engelund (1953) as follows:

$$\alpha = \alpha_0 \frac{(1-n)^3}{n^2} \frac{\nu}{d^2} \quad , \quad \beta = \beta_0 \frac{1-n}{n^3} \frac{1}{d} \tag{15}$$

where, ν is the kinematic viscosity of water, d is the characteristic diameter of the stone, n is the porosity, and α_0 and β_0 are the material constants. The material constants were investigated by the preliminary experiment. The relationship between the pressure difference and the discharge of the seepage was obtained in the experiment, and the constants were determined as $\alpha_0 = 2100$ and $\beta_0 = 1.5$. The pressure difference due to the water level difference between the inside and outside of breakwater was given at both ends of the computational domain.

A Reynolds stress model was used as a relatively high accuracy turbulence model among the RANS models, since preliminary computation results showed that the degree of diffusion of the

impinging jet was influenced by the turbulence model. The Reynolds stress model improved the diffusion of the jet comparing to the result with a standard k-ε turbulence model. Also there was a problem that excessive turbulence was generated at the surface of the rubble mound when the jet flowed along the rubble mound. In this study, the turbulence inside the rubble mound was set to zero as a countermeasure for this problem. Fig. 15 shows the comparison of the computed flow field with the measured one in a steady state. The measured data was obtained by using an electromagnetic current meter, and was averaged for 20 seconds. The computed result with the countermeasures mentioned above adequately reproduced the measured flow field.

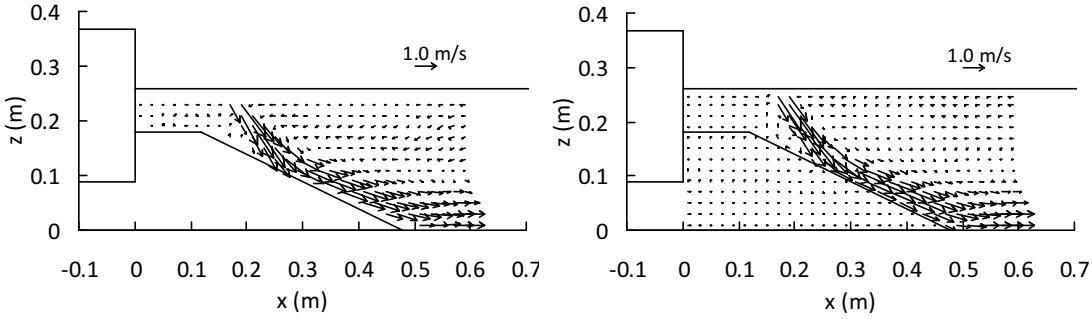

Figure 15. Comparison of measured and computed flow field, h_1 = 9 cm.

Analysis of the stability of armor block

The stability of the armor blocks was analyzed based on the fluid force acting on each block. An experimental case was selected where the overflow jet impinged on the shoulder of the mound. Fig. 16 shows the experimental result of this case. When the overflow depth was 5 cm, the blocks at the shoulder (block No. 3) were overturned. Fig. 17 shows the computed flow field and fluid force acting on each block. A large force acted on the block at the shoulder (block No. 3). The stability of this block was judged by the balance of moment. In this analysis, only the fluid force, buoyant force, and self-weight were considered, but other forces such as the friction force between blocks were disregarded. The condition of the occurrence of overturning was expressed as follows:

$$F_x a_H + F_z a_V + M_y > (\rho_r - \rho_w) V g a_V \qquad (16)$$

where, F_x is the horizontal fluid force, F_z is the vertical fluid force, M_y is the moment due to the fluid force, a_H and a_V are the arm length, ρ_r is the density of the armor unit, ρ_w is the density of water, and V is the volume of the armor block (see Fig. 18). The resistance moment, which is the right hand side of Eq. (16) was calculated to be 49.0 N·mm in this case. Meanwhile, the acting moment, which is the left hand side of Eq. (16), was calculated to be 42.4 N·mm when the overflow depth was 4 cm, 54.8 N·mm when the overflow depth was 5 cm. Thus, this result agreed with the experimental one. Further validation is required, but this numerical analysis will be able to be applied for identification of the weak point in a structure, as well as the prediction of the stability of the armor blocks.

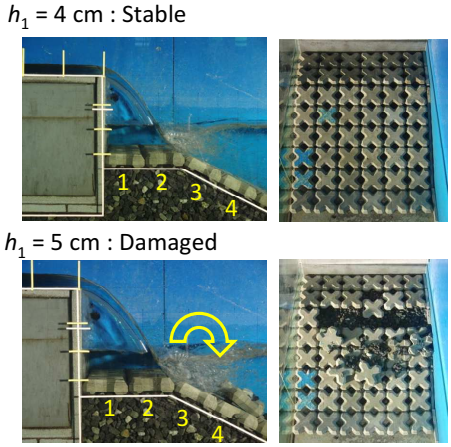

Figure 16. Experimental result, X-block, mass = 254 g

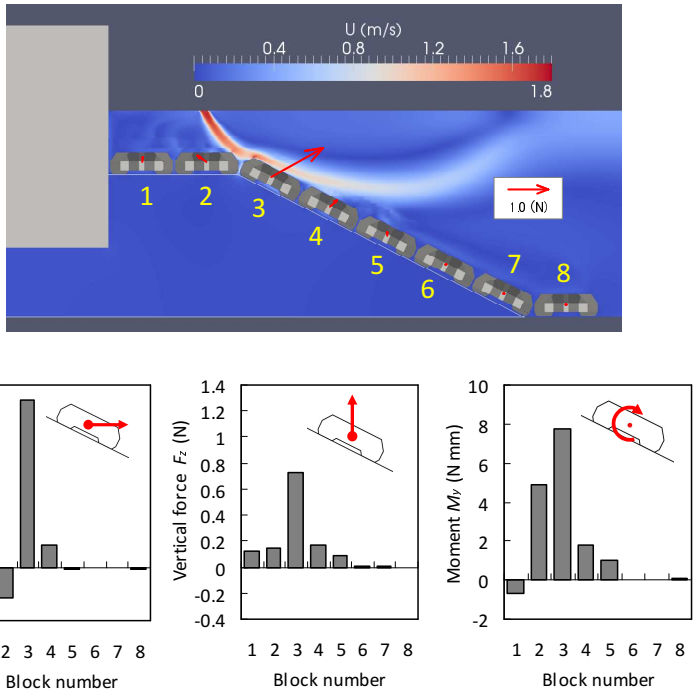

Figure 17. Computed flow field and fluid force acting on each block.

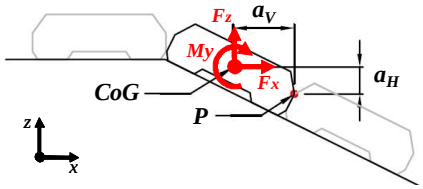

Figure 18. Analysis of the balance of moment of the block.

CONCLUSIONS

A practical design method of armor units to cover a rubble mound at the rear side of a caisson breakwater against tsunami overflow has been proposed. The features of this method are summarized as follows:

- The overflow depth is used to represent the external force. This enables the estimation of the required mass of the armor units to be done more robustly and easily than in the conventional method based on the flow velocity.
- Two formulae are used corresponding to the two failure modes, overturning and sliding.
- This method takes into account the influence of the impingement position of an overflow jet and the influence of the harbor-side water depth. These factors are important for armor stability.

The stability numbers N_{S1} and N_{S2} for each armor unit were determined through experiments conducted in a wide range of conditions. The estimated results by this method have agreed well with the experimental ones.

Numerical analysis was also carried out aiming to evaluate the stability in the case of beyond the range of experimental conditions. The computational method was validated by comparing a computed flow field with a measured one. The stability of the armor blocks were investigated targeting the case where the overflow jet impinged on the shoulder of the mound. The stability judged by the computed fluid forces acting on the armor blocks agreed with the experimental result.

REFERENCES

Arikawa, T., M. Sato, K. Shimosako, T. Tomita, G. Yeom, and T. Niwa. 2013. Failure mechanism and resiliency of breakwaters under tsunami, *Technical Note of the Port and Airport Research Institute*, No. 1269 (in Japanese).

Bricker, J.D., H. Takagi, and J. Mitsui. 2013. Turbulence model effects on VOF analysis of Breakwater overtopping during the 2011 Great East Japan Tsunami, *Proceedings of the 2013 IAHR World Congress*, Chengdu, Sichuan, China, paper A10153.

Coastal Engineering Research Center. 1977. Shore Protection Manual, U.S. Army Corps of Engineers, U.S. Government Printing Office, Vol. II, 7_213-7_216.

Engelund, F. 1953. On the laminar and turbulent flows of ground water through homogeneous sand, *Transactions of the Danish Academy of Technical Sciences*, Vol. 3, No. 4.

Hamaguchi, M., S. Kubota, A. Matsumoto, M. Hanzawa, M. Yamamoto, H. Moritaka, and K. Shimosako. 2007. Hydraulic stability of new flat type armor block with very large openings for use in composite breakwater rubble mound protection, *Proceedings of Coastal Structures 2007*, ASCE, 116-127.

Hom-ma, M. 1940a. Discharge coefficient on overflow weir (part-1), *JSCE Magazine*, *Civil Engineering*, Vol. 26, No. 6, 635-645 (in Japanese).

Hom-ma, M. 1940b. Discharge coefficient on overflow weir (part-2), *JSCE Magazine*, *Civil Engineering*, Vol. 26, No. 9, 849-862 (in Japanese).

Kubota, S., M. Hamaguchi, A. Matsumoto, M. Hanzawa, and M. Yamamoto. 2008. Wave force and stability of new flat type concrete block with large openings for submerged breakwaters, *Proceedings of 31st International Conference on Coastal Engineering*, ASCE, 3423-3435.

Ministry of Land, Infrastructure, Transport and Tourism, Port and Harbor Bureau. 2013. Design guideline of breakwaters against tsunami (in Japanese).

Mitsui, J., S. Maruyama, A. Matsumoto, and M. Hanzawa. 2012. Stability of armor units covering harbor-side rubble mound of composite breakwater against tsunami overflow, *Journal of JSCE, Ser. B2* (*Coastal Engineering*), Vol. 68, No. 2, I_881-I_885 (in Japanese).

OpenCFD Ltd. OpenFOAM User Guide version 2.0.1, http://www.openfoam.com

Van der Meer, J.W. 1988. Stability of cubes, tetrapods and accropode, *Proceedings of Conf. Breakwaters '88*, 71-80.